# Thermally induced formation of metastable nanocomposites in amorphous Cr-Zr-O thin films deposited using reactive ion beam sputtering

Rafaja, D.; Wüstefeld, C.; Abrasonis, G.; Braeunig, S.; Baehtz, C.; Hanzig, F.; Dopita, M.; Krause, M.; Gemming, S.;

Originally published:

June 2016

**Thin Solid Films 612(2016), 430-436**

DOI: https://doi.org/10.1016/j.tsf.2016.06.038

Perma-Link to Publication Repository of HZDR:

https://www.hzdr.de/publications/Publ-23966

# Thermally induced formation of metastable nanocomposites in amorphous Cr-Zr-O thin films deposited using reactive ion beam sputtering

David Rafaja, Christina Wüstefeld, Gintautas Abrasonis, Stefan Braeunig, Carsten Baehtz, Florian Hanzig, Milan Dopita, Matthias Krause, Sibylle Gemming

PII: S0040-6090(16)30282-6
DOI: doi: 10.1016/j.tsf.2016.06.038
Reference: TSF 35278

To appear in: *Thin Solid Films*

Received date: 12 February 2016
Revised date: 21 March 2016
Accepted date: 18 June 2016

# Thermally induced formation of metastable nanocomposites in amorphous Cr-Zr-O thin films deposited using reactive ion beam sputtering

David Rafaja [a,*)], Christina Wüstefeld [a)], Gintautas Abrasonis [b)], Stefan Braeunig [a)], Carsten Baehtz [b)], Florian Hanzig [a)], Milan Dopita [a,c)], Matthias Krause [b)], Sibylle Gemming [b,d)]

a) Institute of Materials Science, Freiberg University of Technology, D-09599 Freiberg, Germany

b) Helmholtz-Zentrum Dresden-Rossendorf, P.O. Box 510119, D-01314 Dresden, Germany

c) Present address: Dept. of Condensed Matter Physics, Faculty of Mathematics and Physics, Charles University, CZ-121 16 Prague, Czech Republic

d) Institute of Physics, Technische Universität Chemnitz, D-09126 Chemnitz, Germany

## Abstract

Successive crystallization of amorphous Cr-Zr-O thin films, formation of the $(Cr,Zr)_2O_3/(Zr,Cr)O_2$ nanocomposites and the thermally induced changes in the hexagonal crystal structure of metastable $(Cr,Zr)_2O_3$ were investigated by means of in situ high-temperature synchrotron diffraction experiments up to 1100°C. The thin films were deposited at room temperature by using reactive ion beam sputtering, and contained 3 – 15 at.% Zr. At low Zr concentrations, chromium-rich $(Cr,Zr)_2O_3$ crystallized first, while the crystallization of zirconium-rich $(Zr,Cr)O_2$ was retarded. Increasing amount of zirconium shifted the onset of crystallization in both phases to higher temperatures. For 3 at.% of zirconium in amorphous Cr-Zr-O, $(Cr,Zr)_2O_3$ crystallized at 600°C. At 8 at.% Zr in the films, the crystallization of $(Cr,Zr)_2O_3$ started at 700°C. At 15 at.% Zr, the Cr-Zr-O films remained amorphous up to the annealing temperature of 1000°C. Metastable hexagonal $(Cr,Zr)_2O_3$ accommodated up to ~3 at.% Zr. Excess of zirconium formed tetragonal zirconia, which was stabilized by chromium.

***Keywords***

* Corresponding author. E-mail address: rafaja@ww.tu-freiberg.de (D. Rafaja)

Metastable oxides, In situ synchrotron diffraction, Crystallization, Reactive ion beam sputtering, Rutherford backscattering spectrometry

## 1. Introduction

Chromium oxide thin films are steadily in focus of interest because of their specific optical [1-4], magnetic [5, 6] and mechanical properties [7], which can further be tailored and improved if $Cr_2O_3$ is doped by selected metallic elements or prepared in a nanostructured form. In its stoichiometric form, $Cr_2O_3$ crystallizes in the corundum-type structure, in which the chromium and oxygen atoms occupy the Wyckoff positions 12c and 18e, respectively. Oyama *et al.* [8] doped chromium oxide by titanium and reported that the corundum-type crystal structure of $Cr_2O_3$ can accommodate up to approximately 10 at.% Ti by forming $(Cr_{1.5}Ti_{0.5})O_3$. From the analysis of the X-ray diffraction data, the authors concluded that titanium atoms replace the chromium atoms in the host structure of $Cr_2O_3$. Later on, the same authors showed that chromium atoms in the corundum-type crystal structure of $Cr_2O_3$ can also be replaced by vanadium in the whole composition range between $Cr_2O_3$ and $V_2O_3$ [9].

Bühler *et al.* [10] investigated the incorporation of molybdenum into the crystal structure of $Cr_2O_3$ and concluded that $Cr_{2-2x}Mo_xO_3$ can accommodate up to 6.6 at.% Mo. In contrast to Ti and V, which were assumed to replace chromium atoms at their intrinsic Wyckoff position 12c [8, 9], the Mo atoms in $Cr_{2-2x}Mo_xO_3$ were shown to occupy the originally empty Wyckoff position 6b [10]. The doping of $Cr_2O_3$ with tin was studied by Ayub *et al.* [11], who have shown that Sn atoms partially replace chromium atoms located at the Wyckoff position 12c and partially occupy the originally empty sites 6b.

In the pseudo-binary system $ZrO_2$–$Cr_2O_3$, especially the $ZrO_2$-rich part was investigated in detail. According to Jerebtsov *et al.* [12], the cubic zirconia (c-$ZrO_2$), which is thermodynamically stable between 2377°C and 2710°C, can be stabilized to 1840°C by up to 25 mass %

$Cr_2O_3$. Tetragonal zirconia (t-$ZrO_2$) can accommodate up to 9 mass % $Cr_2O_3$ in the temperature range between 1115°C and 1840°C. Between 1840°C and 2377°C that is the limit of the thermal stability of stoichiometric t-$ZrO_2$, the maximum content of $Cr_2O_3$ in t-$ZrO_2$ decreases successively. Tetragonal $ZrO_2$ without chromium oxide transforms to monoclinic zirconia (m-$ZrO_2$) below 1165°C, t-(Zr,Cr)$O_2$ with 9 mass % $Cr_2O_3$ transforms to m-(Zr,Cr)$O_2$ below 1115°C.

Several authors reported that the incorporation of chromium into the crystal structure of zirconia stabilizes the tetragonal structure of $ZrO_2$ down to room temperature [13-15]. Štefanić *et al.* [13] prepared chromium-stabilized t-$ZrO_2$ from amorphous precursors, which were calcined for 3 h at different temperatures between 500°C and 1000°C. With increasing molar fraction of $CrO_{1.5}$ in $ZrO_2$, the tetragonal phase of (Zr,Cr)$O_2$ remained stable despite annealing at high temperatures. For more than 0.1 mol $CrO_{1.5}$ incorporated in $ZrO_2$, t-(Zr,Cr)$O_2$ was stable upon annealing up to 800°C. Ray *et al.* [14, 15] prepared metastable t-(Zr,Cr)$O_2$ from a polymer precursor, which was calcined between 250°C and 900°C for 2 hours. At the chromium concentrations of 10 at.%, t-(Zr,Cr)$O_2$ was stabilized in the whole temperature range between 250°C and 900°C. However, a longer annealing at 900°C or higher temperatures destabilized the tetragonal (Zr,Cr)$O_2$ and led to a concurrent formation of thermodynamically stable m-$ZrO_2$ and hexagonal $Cr_2O_3$. At 20 at.% Cr contained in (Zr,Cr)$O_2$, the hexagonal $Cr_2O_3$ segregated from the metastable solid solution during the calcination already at 800°C and appeared together with t-(Zr,Cr)$O_2$. Still, no monoclinic $ZrO_2$ was observed.

In contrast to the large solubility of chromium in $ZrO_2$, the solubility of $ZrO_2$ in thermodynamically stable hexagonal $Cr_2O_3$ is extremely low [16]. Still, Spitz *et al.* [7] found that the host structure of hexagonal (corundum-type) $(Cr,Zr)_2O_3$ in their Cr-Zr-O thin films accommodates up to 12 at.% of zirconium. These films were deposited by using radio-frequency (rf) magnetron sputtering on heated substrates ($T_{sub}$ = 500°C). In the thin films containing 18 at.%

Zr, 20 at.% Cr and 62 at.% O, the authors observed a single-phase cubic solid solution and concluded from their results that chromium is completely dissolved in the structure of c-$(Zr,Cr)O_2$. At higher Zr contents, two phases were identified in the rf magnetron deposited Zr-Cr-O thin films, i.e., t-$(Zr,Cr)O_2$ and m-$(Zr,Cr)O_2$.

In our study, the formation of crystalline phases in originally amorphous chromium-rich Cr-Zr-O thin films and the thermally induced changes in the crystal structures of metastable hexagonal $(Cr,Zr)_2O_3$ were investigated during the annealing up to 1100°C. The films were deposited on unheated thermally oxidized silicon substrates by using ion beam co-sputtering from zone Cr-Zr targets. The Zr content in the films was between 3 and 15 at.%. In order to produce oxide films, oxygen was directed to the growing film during the deposition process. The crystallization process and the changes in the crystal structure of h-$(Cr,Zr)_2O_3$ were followed in in-situ synchrotron diffraction experiments. A structure model is presented, which is capable of describing the location and amount of zirconium atoms in the corundum-type host structure of $Cr_2O_3$.

## 2. Experimental details

Thin films of chromium zirconium oxides were deposited using reactive ion beam sputtering from zone Cr-Zr targets on (001)-oriented thermally oxidized silicon single crystals [17, 18]. Argon ions were generated in a Kaufman ion source with a diameter of 3 cm (IonTech Inc., Fort Collins, USA) and accelerated by the voltage of 1000 V. The total ion beam sputtering current was kept constant at (40 ± 1) mA during the whole deposition process (6 hours). A zone Cr-Zr target was placed at a distance of 17 cm from the Kaufman ion source and at a distance of 18 cm from the substrate holder. The target was inclined with respect to the argon ion beam; the angle between the impinging Ar ions and the target normal direction was ap-

proximately 22°. The main part of the target was a chromium disc (99.95 %) with a diameter of 15 cm that was covered in the middle by differently wide strips (5, 10 or 15 mm), which were made from zirconium having the same purity like the chromium target. As the area of the target irradiated by the argon ion beam was the same in all deposition runs, the width of the Zr strip controlled the [Zr]/([Cr]+[Zr]) ratio in the respective sample. Prior to the deposition process, the surface of the target and the Zr strip were cleaned by argon ions.

The base pressure in the deposition chamber was $2.9 \times 10^{-5}$ Pa, rising to $9.1 \times 10^{-3}$ Pa due to the Ar supply into the ion gun. In order to avoid interference with the sputter process, oxygen was supplied directly to the growing films. The oxygen flow of 2 sccm that was used for deposition of all samples further increased the pressure in the deposition chamber up to $1.2 \times 10^{-2}$ Pa. Although the substrates were not heated during the deposition process, the kinetic energy of the impinging atoms raised the substrate temperature to (57 ± 4) °C. The thickness of the thin films was approx. 600 nm as determined by profilometry.

Chemical composition of the as-deposited Cr-Zr-O films was determined by using Rutherford backscattering spectrometry (RBS) with $^{4}He^{+}$ ions that had the energy of 1.7 MeV. The measured RBS spectra were analyzed by using the SIMNRA code [19, 20]. The phase and structure analyses were performed using in situ high-temperature synchrotron diffraction experiments at the Rossendorf beamline (ROBL@BM20, ESRF Grenoble). The diffraction patterns were acquired in the glancing-angle diffraction geometry at the angle of incidence of 0.7° and at the wavelength of 0.10796(4) nm. The wavelength of the synchrotron radiation was calibrated through diffraction measurements, which were done on an external standard. At the above wavelength and for all chemical compositions of the Cr-Zr-O thin films under study, the applied angle of incidence was beyond the edge of the total external reflection, thus the whole thickness of the thin films was irradiated by the synchrotron primary beam. For each sample, a preliminary diffraction measurement at room temperature and twelve measurements

between 500°C and 1100°C were carried out. The temperature step was 100°C. In order to be able to correct the measured lattice parameters for thermal expansion, diffraction measurements at 100°C were interposed between the high-temperature measurements as suggested in [21]. All in situ high-temperature diffraction measurements were performed in a vacuum chamber at the residual pressure between $2 \times 10^{-4}$ Pa and $1.4 \times 10^{-5}$ Pa. The window of the chamber was covered by a kapton foil.

## 3. Results and discussion

### *3.1 Thermally induced crystallization of Cr-Zr-O films*

The RBS analysis revealed that the as-deposited samples contained (2.9 ± 0.1) at.%, (8.0 ± 0.2) at.% and (14.8 ± 0.5) at.% of zirconium. In the following, these samples are denoted as Zr3CrO, Zr8CrO and Zr15CrO, respectively. With increasing concentration of zirconium, the concentration of chromium decreased as expected. The measured oxygen content was 64 at.% in all samples (within the experimental accuracy) and thus higher than expected for a mixture of two stoichiometric compounds, $Cr_2O_3$ and $ZrO_2$, in the investigated range of Zr concentrations (cf. Table 1). This finding indicates that the as-deposited samples do not contain a mixture of $Cr_2O_3$ and $ZrO_2$, i.e., $Cr_{2-2x}Zr_xO_{3-x}$, but a solid solution of chromium, zirconium and oxygen. The oxygen deficiency was assumed because of the charge balance.

This result was supported by X-ray diffraction, which identified the as-deposited thin films as amorphous. At temperatures above 500°C, the Cr-Zr-O films began to crystallize. However, the onset of crystallization was strongly dependent on the overall zirconium content in the thin films. Thin film Zr3CrO crystallized rapidly between 500°C and 600°C (Fig. 1). The crystallization started by the formation of hexagonal $(Cr,Zr)_2O_3$ having the space group $R\bar{3}c$. Tetragonal $(Zr,Cr)O_2$ (SG $P4_2/nmc$) formed as a minor phase first above 900°C. The crystalli-

zation of t-$(Zr,Cr)O_2$ was evidenced from the presence of the very weak diffraction line 101 located at $2\theta = 21°$. Even after annealing at 1100°C, h-$(Cr,Zr)_2O_3$ was the dominant phase in this film. Upon annealing, the size of the $(Cr,Zr)_2O_3$ crystallites, which was determined by using the Williamson & Hall method [22], increased from 60 nm (at 600°C) to 80 nm (at 1100°C). The amount of t-$(Zr,Cr)O_2$ was low, thus the size of the t-$(Zr,Cr)O_2$ crystallites could not be determined reliably.

In the thin film Zr8CrO, the onset of crystallization and the formation of h-$(Cr,Zr)_2O_3$ was observed between 600°C and 700°C. As it can be seen from Fig. 2, the first pronounced diffraction lines were 110 ($2\theta = 25.0°$), 300 ($2\theta = 44.1°$) and 220 ($2\theta = 51.4°$), which correspond to the prismatic lattice planes in the crystal structure of h-$(Cr,Zr)_2O_3$. This suggests that the atomic ordering starts between 600°C and 700°C within the basal lattice planes, whereas the long-range periodicity in the ***c*** direction establishes at 1000°C. At the temperature of 1000°C, also nanocrystalline t-$(Zr,Cr)O_2$ was formed. Between 1000°C and 1100°C, the size of h-$(Cr,Zr)_2O_3$ crystallites increased from 20 nm to 40 nm, the size of t-$(Zr,Cr)O_2$ crystallites from 10 to 25 nm.

The onset of the h-$(Cr,Zr)_2O_3$ crystallization was further retarded by increasing the overall Zr content to (14.8 ± 0.5) at. %. In sample Zr15CrO, hexagonal $(Cr,Zr)_2O_3$ and tetragonal $(Zr,Cr)O_2$ crystallized concurrently between 900°C and 1000°C (Fig. 3). The size of h-$(Cr,Zr)_2O_3$ and t-$(Zr,Cr)O_2$ crystallites was about 30 nm and 20 nm, respectively.

From these results, it can be concluded that a higher Zr content in originally amorphous Cr-Zr-O thin films retards the crystallization of hexagonal $(Cr,Zr)_2O_3$ and facilitates the formation of t-$(Zr,Cr)O_2$, which inhibits the growth of the h-$(Cr,Zr)_2O_3$ crystallites.

*3.2 Thermal stability of metastable hexagonal $(Cr,Zr)_2O_3$*

The Rietveld analysis [23, 24] of measured XRD patterns supported by the difference Fourier synthesis method [25] has shown that the Wyckoff position 6b, which is usually vacant in the corundum-type crystal structure of $Cr_2O_3$, is partially occupied in our thin films. For both methods, i.e., for the Rietveld analysis and for the difference Fourier synthesis, the Fullprof suite [26] was employed. In analogy with the structure model of Bühler *et al.* [10], it was assumed that the Wyckoff position 6b in h-$(Cr,Zr)_2O_3$ is partially occupied by zirconium. The partial occupancy of this Wyckoff position in the space group $R\bar{3}c$ affects the intensities of several diffraction lines. Most pronounced is the change of the intensity of the diffraction line 006 that is very weak for ideal $Cr_2O_3$ structure but much stronger if the Wyckoff site 6b is partially occupied by zirconium (cf. Fig. 4).

The results of the Rietveld refinement [26] performed with this structure model have shown that the occupancy of the Wyckoff position 6b by Zr atoms and thus the Zr concentration in h-$(Cr,Zr)_2O_3$ depend strongly on the overall zirconium concentration in individual samples (Fig. 5). At low overall Zr concentrations (2.9 and 8.0 at.%), the maximum occupancy of the Wyckoff position 6b by zirconium (12 % and 16 %, respectively) slightly increased with the overall Zr concentration in the sample. On the other hand, the amount of Zr atoms embedded in the crystal structure of h-$(Cr,Zr)_2O_3$ did not change significantly with annealing temperature in samples Zr3CrO and Zr8CrO. At the highest overall Zr concentration in sample Zr15CrO (14.8 at.%), less than 5 % of the Wyckoff positions 6b were occupied by zirconium. In contrast to samples Zr3CrO and Zr8CrO, where the Zr atoms resided in the crystal structure of h-$(Cr,Zr)_2O_3$ up to 1100°C, the Zr atoms in sample Zr15CrO successively left the host structure of h-$Cr_2O_3$ with increasing temperature. At 1100°C, hexagonal $(Cr,Zr)_2O_3$ was almost completely free of zirconium.

In order to enable a straightforward comparison between the chemical composition of h-$(Cr,Zr)_2O_3$ obtained from the Rietveld analysis and the overall chemical composition measured using RBS, the refined occupancies of the Wyckoff position 6b were converted into Zr concentrations in h-$(Cr,Zr)_2O_3$ according to Eq. (1):

$$[\mathrm{Zr}] = \frac{6 \times occ(\mathrm{Zr})}{6 \times occ(\mathrm{Zr}) + 12 \times occ(\mathrm{Cr}) + 18 \times occ(\mathrm{O})} \quad (1)$$

The numerical factors in Eq. (1) reproduce the number of the Wyckoff positions 6b, 12c and 18e, respectively. Within the applied model, the Wyckoff position 18e was assumed to be fully occupied by oxygen, whereas the occupancies of the Wyckoff positions 6b and 12 c were linked to fulfil the relationship *occ*(Cr) = 1 – *occ*(Zr). Consequently, equation (1) yields

$$[\mathrm{Zr}] = \frac{6 \times occ(\mathrm{Zr})}{-6 \times occ(\mathrm{Zr}) + 12 + 18} = \frac{occ(\mathrm{Zr})}{5 - occ(\mathrm{Zr})} \quad (2)$$

For small amounts of zirconium in the host structure of h-$Cr_2O_3$, i.e. for small *occ*(Zr), the amount of zirconium [Zr] is approximately equal to *occ*(Zr)/5, see Fig. 5.

The maximum occupancy of the Wyckoff position 6b in sample Zr3CrO (12 %) corresponds to 2.5 at.% Zr in hexagonal $Cr_{2-2x}Zr_xO_{3-x}$. This amount of Zr approaches the overall concentration of zirconium, which was measured in this sample by RBS (2.9 at.%). This finding agrees very well with the result of quantitative phase analysis, which revealed that the amount of t-$(Zr,Cr)O_2$ is below 1 mol % in sample Zr3CrO up to the annealing temperature of 1100°C. After annealing at 1100°C and cooling to 100°C (Fig. 6), sample Zr3CrO contained, according to the Rietveld analysis [26], 2.5 mol % of t-$(Zr,Cr)O_2$ and 97.5 mol % of h-$Cr_{2-2x}Zr_xO_{3-x}$. This $Cr_{2-2x}Zr_xO_{3-x}$ accommodated 2.1 at.% Zr.

In sample Zr8CrO, hexagonal $Cr_{2-2x}Zr_xO_{3-x}$ contained up to 3.2 at.% Zr (at 1000°C, see Fig. 5) despite the overall Zr concentration of 8.0 at.% (Table 1). The remainder of Zr formed t-

$(Zr,Cr)O_2$. With increasing temperature of the annealing process, the amount of Zr incorporated in $Cr_{2-2x}Zr_xO_{3-x}$ decreased. In return, the amount of t-$(Zr,Cr)O_2$ in the sample increased (Fig. 6). However, even after annealing at 1100°C and cooling to 100°C it was far below 37 mol % t-$ZrO_2$ that would be the amount of t-$ZrO_2$ in a mixture of binary phases, $Cr_2O_3$ and $ZrO_2$, in a sample containing 8.0 at.% Zr and 27.0 at.% Cr (see below).

In sample Zr15CrO, the occupancy of the Wyckoff position 6b by zirconium was about 4 % at the beginning of the crystallization process. This occupancy corresponds to a Zr content in h-$Cr_{2-2x}Zr_xO_{3-x}$ below 1 at.% (Fig. 5). At the end of the annealing sequence, i.e. at 100°C after annealing at 1100°C, the hexagonal phase in sample Zr15CrO accommodated only 0.4 at.% Zr. The low concentrations of Zr in h-$Cr_{2-2x}Zr_xO_{3-x}$ concluded for sample Zr15CrO are corroborated by high amounts of t-$(Zr,Cr)O_2$, which are very close to the phase fractions calculated for a mixture of $Cr_2O_3$ and $ZrO_2$ (dotted line in Fig. 6).

The maximum mole fractions of $ZrO_2$ (dashed lines in Fig. 6) were calculated using

$$x\,(\mathrm{mol\ ZrO_2}) = \frac{2\,[\mathrm{Zr}]/([\mathrm{Zr}]+[\mathrm{Cr}])}{[\mathrm{Zr}]/([\mathrm{Zr}]+[\mathrm{Cr}])+1}\,, \tag{3}$$

under the assumption that the deposited Cr-Zr-O films fully decompose into $Cr_2O_3$ and $ZrO_2$. The concentrations of Zr and Cr at the right-hand side of Eq. (3) were taken from the RBS analysis (Table 1). The corresponding amounts of $ZrO_2$ in samples Zr3CrO, Zr8CrO and Zr15CrO are 15 mol %, 37 mol % and 60 mol %, respectively.

As already discussed above, the observed difference between the phase composition obtained from the Rietveld refinement [26] and the phase composition, which was calculated for a mixture of binary phases, correlates very well with the amount of zirconium incorporated in h-$Cr_{2-2x}Zr_xO_{3-x}$. The Zr atoms, which are embedded in the structure of $Cr_{2-2x}Zr_xO_{3-x}$, do not form

t-$(Zr,Cr)O_2$ but contribute to the diffraction pattern of h-$(Cr,Zr)_2O_3$ from the point of view of the XRD phase analysis.

Accordingly, the molar fractions of t-$(Zr,Cr)O_2$ in samples Zr3CrO and Zr8CrO that were obtained from the XRD phase analysis are lower than expected (Fig. 6), because a significant amount of Zr is incorporated in the crystal structure of h-$Cr_{2-2x}Zr_xO_{3-x}$ (Fig. 5). In sample Zr15CrO, the molar fraction of t-$(Zr,Cr)O_2$ approaches the expected quantity, as hexagonal $Cr_{2-2x}Zr_xO_{3-x}$ contains only a small amount of Zr. The slightly lower content of t-$(Zr,Cr)O_2$ measured in sample Zr15CrO at 1100°C is associated with a higher content of Zr in $Cr_{2-2x}Zr_xO_{3-x}$.

The direct correlation between the phase composition and the amount of zirconium in h-$Cr_{2-2x}Zr_xO_{3-x}$ that have been obtained from the XRD analysis is violated if a part of Cr atoms is incorporated in t-$(Zr,Cr)O_2$ or if some of the metallic atoms are trapped in the remnants of the amorphous phase. According to references [13-15], chromium belongs to the elements, which stabilize the tetragonal structure of zirconia. Therefore, it can be assumed that the tetragonal phase in all samples under study contains chromium as a stabilizing element.

### *3.3 Thermal expansion of metastable $(Cr,Zr)_2O_3$*

The incorporation of Zr atoms into the crystal structure of hexagonal $Cr_2O_3$ is expected to modify additionally the lattice parameters and the thermal expansion of h-$Cr_{2-2x}Zr_xO_{3-x}$. The lattice parameters were determined from the in situ synchrotron diffraction data by using the MAUD software [27]. The MAUD software was used because it can determine stress-free lattice parameters in thin films that are under macroscopic stress. In our samples, the possible reasons for the macroscopic lattice strain are the different thermal expansion coefficients of the substrate and the film, the formation of the crystal structures (h-$(Cr,Zr)_2O_3$ and t-

$(Zr,Cr)O_2$) during the crystallization of amorphous Cr-Zr-O and the segregation of the metallic elements.

The stress-free lattice parameters of metastable h-$(Cr,Zr)_2O_3$, which are summarized in Fig. 7, were calculated with the elastic constants $E(Cr_2O_3)$ = 311 GPa and $\nu(Cr_2O_3)$ = 0.26 from Ref. [28] and with $E(ZrO_2)$ = 212 GPa and $\nu(ZrO_2)$ = 0.314 from Ref. [29]. It was assumed that the residual stress is equi-biaxial. In almost all samples under study, the stress-free lattice parameters of h-$(Cr,Zr)_2O_3$ were larger than the lattice parameters of pure $Cr_2O_3$ ($a$ = 0.49607 nm, $c$ = 1.3599 nm [30]). The observed expansion of the elementary cell is a consequence of the incorporation of Zr atoms into the elementary cell of $Cr_2O_3$. A similar effect was reported by Oyama *et al.* in [8] for $(Cr,Ti)_2O_3$. At 100°C (after cooling from the respective annealing temperature) where the effect of the thermal expansion on the lattice parameters is much weaker than at the annealing temperatures, the largest stress-free lattice parameters were observed for samples Zr3CrO and Zr8CrO with the highest occupancies of the Wyckoff position 6b by zirconium. The stress-free lattice parameters of h-$(Cr,Zr)_2O_3$ in sample Zr15CrO, which contained less than 1 at.% Zr, are substantially lower and approach the intrinsic values of $Cr_2O_3$ [30]. The lattice parameters of h-$(Cr,Zr)_2O_3$ containing 0.2 at.% Zr (sample Zr15CrO at 100°C after annealing at 1100°C) were almost identical with the lattice parameters of Zr-free $Cr_2O_3$ [30].

Figure 7 shows additionally the changes in the lattice parameters, which are expected during the thermal cycling as a consequence of a constant (temperature-independent) thermal expansion that is characterized by the thermal expansion coefficients $\alpha_a = 7.60 \times 10^{-6}\ K^{-1}$ and $\alpha_c = 6.38 \times 10^{-6}\ K^{-1}$ (lines in Fig. 7). The solid line indicates the expanded lattice parameters in sample Zr3CrO, the dashed line the intrinsic lattice parameters of $Cr_2O_3$ [30]. The above thermal expansion coefficients were taken from Fig. 8, where they represent the asymptotic values of $\alpha_a$ and $\alpha_c$ for the highest annealing temperatures. These thermal expansion coeffi-

cients agree very well with the thermal expansion coefficients given by Kudielka [31], i.e., $\alpha_a = 7.85 \times 10^{-6}\ K^{-1}$ and $\alpha_c = 6.38 \times 10^{-6}\ K^{-1}$.

Complete sets of the thermal expansion coefficients calculated from the measured stress-free lattice parameters are displayed in Fig. 8. At the beginning of crystallization, the thermal expansion coefficients are generally lower than in the later phases of the crystallization process. In sample Zr3CrO, the steepest increase of the thermal expansion coefficients of hexagonal $(Cr,Zr)_2O_3$ was observed in the temperature range up to 900°C, where also the Zr content in $Cr_{2-2x}Zr_xO_{3-x}$ slightly increased (cf. Fig. 5). Above 900°C where the Zr content in $Cr_{2-2x}Zr_xO_{3-x}$ was constant in the cooled-down state (100°C), the increase of the thermal expansion coefficients of h-$(Cr,Zr)_2O_3$ decelerates, until a constant thermal expansion was achieved.

In sample Zr8CrO, the thermal expansion coefficients of h-$(Cr,Zr)_2O_3$ were always lower than the intrinsic ones, which is related to a successive segregation of Zr atoms from the crystal structure of $Cr_{2-2x}Zr_xO_{3-x}$. The large changes in the thermal expansion coefficients of h-$(Cr,Zr)_2O_3$ in sample Zr15CrO are caused mainly by the exchange of zirconium between $Cr_{2-2x}Zr_xO_{3-x}$ and the surrounding areas that leads also to large changes in the lattice parameters of h-$(Cr,Zr)_2O_3$. These results show that the thermal expansion coefficient is very sensitive to the consolidation of the crystal structure of $Cr_{2-2x}Zr_xO_{3-x}$ during the annealing and to the incorporation or segregation of Zr atoms into or from the host structure of metastable h-$Cr_{2-2x}Zr_xO_{3-x}$.

## 4. Summary

Amorphous Cr-Zr-O thin films with Zr concentrations between 3 and 15 at.% were deposited in an reactive ion beam co-sputtering process. In all as-deposited samples, the amount of oxygen was higher than it would correspond to a mixture of stoichiometric compounds $Cr_2O_3$ and

$ZrO_2$. During the thermal treatment, the amorphous Cr-Zr-O solid solutions decomposed into metastable h-$(Cr,Zr)_2O_3$ and t-$(Zr,Cr)O_2$, which crystallize in the corundum-type structure and as chromium-stabilized tetragonal zirconia, respectively. The crystallization temperatures are between 600°C and 1000°C depending on the overall Zr content.

Metastable hexagonal $(Cr,Zr)_2O_3$ accommodates up to 3.2 at.% Zr. The zirconium atoms occupy the Wyckoff position 6b, which is vacant in the ideal host structure of $Cr_2O_3$. The excess of zirconium segregates primarily from oversaturated solid solution Cr-Zr-O and forms tetragonal zirconia that is stabilized by the presence of chromium atoms as described in references [13-15]. Accordingly, hexagonal $(Cr,Zr)_2O_3$ crystallizes first if the amount of Zr in the Cr-Zr-O solid solution is below the maximum concentration of Zr in h-$(Cr,Zr)_2O_3$. Higher amount of Zr in the Cr-Zr-O solid solution shifts the onset of crystallization of h-$(Cr,Zr)_2O_3$ to higher temperatures, but it also facilitates a direct and faster formation of tetragonal $(Zr,Cr)O_2$ together with h-$(Cr,Zr)_2O_3$. Concurrent crystallization of h-$(Cr,Zr)_2O_3$ and t-$(Zr,Cr)O_2$ inhibits the growth of crystallites in both phases. However, high overall concentration of Zr in Cr-Zr-O speeds up the formation of t-$(Zr,Cr)O_2$ that leads to a reduction of the Zr content in h-$(Cr,Zr)_2O_3$ and to the transition of metastable h-$(Cr,Zr)_2O_3$ to thermodynamically stable $Cr_2O_3$ at the annealing temperature of 1100°C.

## 5. Conclusions

In this contribution, it was evidenced that thin film nanocomposites containing two metastable crystalline phases, hexagonal $(Cr,Zr)_2O_3$ and tetragonal $(Zr,Cr)O_2$, can be produced from amorphous solid solution Cr-Zr-O via annealing in vacuum. The amorphous solid solutions with different Zr concentrations in Cr-Zr-O were produced by reactive ion beam sputtering on unheated substrates. The hexagonal chromium oxide present in the annealed thin films was

doped with up to 3 at.% Zr. Metastable $Cr_{1.94}Zr_{0.03}O_{2.97}$ survived annealing until 1100°C. The zirconium atoms occupied up to 15 % of the Wyckoff sites 6b, which are empty in the crystal structure of $Cr_2O_3$. It was shown that the microstructure of the h-$(Cr,Zr)_2O_3$/t-$(Zr,Cr)O_2$ nano-composites, and in particular the crystallite size and the concentration of Zr in hexagonal $(Cr,Zr)_2O_3$, can be controlled to some degree through the concentration of zirconium in the Cr-Zr-O solid solution and through the annealing temperature.

***Acknowledgements***

The authors appreciate the allocation of the beamtime at the Rossendorf beamline (ROBL) at the European Synchrotron Radiation Facility in Grenoble. SG acknowledges support by the Initiative and Networking Funds of the president of the Helmholtz Association via the W2/W3 programme and the Virtual Institute Memriox.

**References**

[1] M.G. Hutchins, Selective thin film coatings for the conversion of solar radiation, Surface Technology 20 (1983) 301-320.

[2] P. Hones, M. Diserens, F. Levy, Characterization of sputter-deposited chromium oxide thin films, Surf. Coat. Technol. 120-121 (1999) 277-283.

[3] M.F. Al-Kuhaili, S.M.A. Durrani, Optical properties of chromium oxide thin films deposited by electron-beam evaporation, Optical Materials 29 (2007) 709-713.

[4] H.C. Barshilia, N. Selvakumar, K.S. Rajam, A. Biswas, Magnetic Structure of $Cr_2O_3$, Structure and optical properties of pulsed sputter deposited $Cr_xO_y$/Cr/$Cr_2O_3$ solar selective coatings, J. Appl. Phys. 103 (2008) 023507.

[5] L. M. Corliss, J.M. Hastings, R. Nathans, G. Shirane, Magnetic structure of $Cr_2O_3$, J. Appl. Phys. 36 (1965) 1099-1100.

[6] B. Bhushan, G.S.A.M. Theunissen, X. Li, Tribological studies of chromium oxide films for magnetic recording applications, Thin Solid Films 311 (1997) 67-80.

[7] S. Spitz, M. Stueber, H. Leiste, S. Ulrich, H.J. Seifert, Microstructure evolution of radio-frequency magnetron sputtered oxide thin films in the Cr-Zr-O system, Thin Solid Films 548 (2013) 143-149.

[8] T. Oyama, Y. Iimura, T. Ishii, K. Takeuchi, Synthesis of Cr-Ti binary oxide particles by the laser-induced chain reaction and its crystal structure, Nippon Kagaku Kaishi 1993 (7) (1993) 825-830.

[9] T. Oyama, Y. Iimura, K. Takeuchi, T. Ishii, Synthesis of $(Cr_xV_{1-x})_2O_3$ fine particles by a laser-induced vapor-phase reaction and their crystal structure, J. Mater. Sci. 34 (1999) 439-444.

[10] R. Bühler, J.R. Günter, C. Baerlocher, Preparation and characterization of a new ternary chromium(III)-molybdenum(VI) oxide $Cr_{2-2x}Mo_xO_3$, J. Solid State Chemistry 140 (1998) 350-353.

[11] I. Ayub, F.J. Berry, C. Johnson, D.A. Johnson, E.A. Moore, X. Ren, H.M. Widatallah, Tin-, titanium-, and magnesium-doped $\alpha$-$Cr_2O_3$: characterisation and rationalisation of the structures, Solid State Communications 123 (2002) 141-145.

[12] D.A. Jerebtsov, G.G. Mikhailov, S.V. Sverdina, Phase diagrams of the system $ZrO_2$-$Cr_2O_3$, Ceramics International 27 (2001) 247-250.

[13] G. Štefanić, S. Musić, A. Gajović, Thermal behavior of the amorphous precursors in the $ZrO_2$-$CrO_{1.5}$ system, Journal of Molecular Structure 744-747 (2005) 541-549.

[14] J.C. Ray, P. Pramanik, S. Ram, Formation of $Cr^{3+}$ stabilized $ZrO_2$ nanocrystals in a single cubic metastable phase by a novel chemical route with a sucrose-polyvinyl alcohol polymer matrix, Matter. Lett. 48 (2001) 281-291.

[15] J.C. Ray, C.R. Saha, P. Pramanik, Stabilized nanoparticles of metastable $ZrO_2$ with $Cr^{3+}/Cr^{4+}$ cations: preparation from a polymer precursor and the study of the thermal and structural properties, J. Eur. Ceram. Soc. 22 (2002) 851-862.

[16] S.W. Rhee, M. Hoch, The Zr-Cr-O system, Trans. Metall. Soc. AIME 230 [7] (1964) 1687-1690.

[17] G. Abrasonis, M. Krause, A. Mücklich, K. Sedláčková, G. Radnóczi, U. Kreissig, A. Kolitsch, W. Möller, Growth regimes and metal enhanced 6-fold ring clustering of carbon in carbon–nickel composite thin films, Carbon 45 (2007) 2995-3006.

[18] M. Krause, M. Buljan, A. Mücklich, W. Möller, M. Fritzsche, S. Facsko, R. Heller, M. Zschornak, S. Wintz, J.L. Endrino, C. Baehtz, A. Shalimov, S. Gemming, G. Abrasonis, Compositionally modulated ripples during composite film growth: Three-dimensional pattern formation at the nanoscale, Phys. Rev. 89 (2014) 085418.

[19] M. Mayer, Ion beam analysis of rough thin films, Nuclear Inst. and Methods in Physics Research B 194 (2002) 177-186.

[20] M. Mayer, Improved physics in SIMNRA 7, Nuclear Inst. and Methods in Physics Research B 332 (2014) 176-180.

[21] D. Rafaja, C. Wüstefeld, C. Baehtz, V. Klemm, M. Dopita, M. Motylenko, C. Michotte, M. Kathrein, Effect of internal interfaces on hardness and thermal stability of nanocrystalline $Ti_{0.5}Al_{0.5}N$ coatings, Metal. Mater. Trans. A 42 (2011) 559-569.

[22] G.K. Williamson, W.H. Hall, X-ray line broadening from filed aluminium and wolfram, Acta Metall. 1 (1953) 22-31.

[23] H.M. Rietveld, Line profiles of neutron powder-diffraction peaks for structure refinement, Acta Cryst. 22 (1967) 151-152.

[24] H.M. Rietveld, A profile refinement method for nuclear and magnetic structures, J. Appl. Cryst. 2 (1969) 65-71.

[25] C. Giacovazzo, H.L. Monaco, G. Artioli, D. Viterbo, G. Ferraris, G. Gilli, G. Zanotti, M. Catti: Fundamentals of Crystallography, 2nd edition, IUCr Texts on Crystallography 7, Oxford University Press, 2002, pp. 465.

[26] J. Rodriguez-Carvajal, Recent advances in magnetic structure determination by neutron powder diffraction, Physica B 192 (1993) 55-69.

[27] L. Lutterotti, Total pattern fitting for the combined size-strain-stress-texture determination in thin film diffraction, Nuclear Inst. and Methods in Physics Research B 268 (2010) 334-340.

[28] Y. Wang, H. Fang, C.L. Zacherl, Z. Mei, S. Shang, L.-Q. Chen, P.D. Jablonski, Z.-K. Liu, First-principles lattice dynamics, thermodynamics, and elasticity of $Cr_2O_3$, Surf. Sci. 606 (2012) 1422-1425.

[29] S. Sakaguchi, N. Murayama, Y. Kodama, F. Wakai, The Poisson's ratio of engineering ceramics at elevated temperature, J. Mater. Sci. Letters 10 (1991) 282-284.

[30] R.E. Newnham, Y.M. de Haan, Refinement of the $\alpha$-$Al_2O_3$, $Ti_2O_3$, $V_2O_3$ and $Cr_2O_3$ structures, Z. Krist. 117 (1962) 235-237.

[31] H. Kudielka, Thermal expansion of the isotypic mixed crystal components $Cr_2O_3$ and $\alpha$-$Al_2O_3$ investigated by means of a Seemann-Bohlin camera permitting high intensities, Monatsh. Chem. 103 (1972) 72-80.

**Tables**

Table 1: Concentrations of zirconium, chromium and oxygen measured using Rutherford backscattering spectrometry in the as-deposited amorphous thin films. The last column displays oxygen concentrations that were calculated for the measured concentrations of Zr and Cr assuming a mixture of two stoichiometric compounds, $Cr_2O_3$ and $ZrO_2$, i.e., $Cr_{2-2x}Zr_xO_{3-x}$.

| | Measured concentrations (RBS) | | | Stoichiometric oxygen content |
|---|---|---|---|---|
| Sample | At. % Zr | At. % Cr | At. % O | At. % O |
| Zr3CrO | 2.9 ± 0.1 | 32.2 ± 0.8 | 63.9 ± 1.0 | 60.6 |
| Zr8CrO | 8.0 ± 0.2 | 27.0 ± 0.3 | 64.0 ± 0.4 | 61.7 |
| Zr15CrO | 14.8 ± 0.5 | 19.4 ± 0.2 | 64.2 ± 0.4 | 63.2 |

**Figure captions**

Figure 1: A part of the X-ray diffraction patterns measured in as-deposited sample Zr3CrO (AD) and during annealing at the indicated temperatures. The intensities are shown on logarithmic scale to enhance the weak reflections. Straight vertical lines mark the positions of the diffraction lines from h-$(Cr,Zr)_2O_3$ (solid lines) and t-$(Zr,Cr)O_2$ (dotted lines).

Figure 2: A part of the X-ray diffraction patterns measured in as-deposited sample Zr8CrO (AD) and during annealing at the indicated temperatures. The solid lines mark the positions of the diffraction lines from h-$(Cr,Zr)_2O_3$, the dotted lines the positions of the diffraction lines from t-$(Zr,Cr)O_2$.

Figure 3: A part of the X-ray diffraction patterns measured in as-deposited sample Zr15CrO (AD) and during annealing at the indicated temperatures. The solid lines mark the positions of the diffraction lines from h-$(Cr,Zr)_2O_3$, the dotted lines the positions of the diffraction lines from t-$(Zr,Cr)O_2$.

Figure 4: A part of the measured X-ray diffraction patterns (small circles) and the corresponding Rietveld fits (solid lines) for samples Zr3CrO, Zr8CrO and Zr15CrO (from bottom to top) that were cooled to 100°C after annealing at 1100°C. The dotted lines and the corresponding diffraction indices label the diffraction lines from hexagonal $(Cr,Zr)_2O_3$.

Figure 5: Occupancy of the Wyckoff position 6b in hexagonal $Cr_{2-2x}Zr_xO_{3-x}$ by zirconium as obtained from the Rietveld refinement of the measured diffraction patterns.

Figure 6: Content of tetragonal $(Zr,Cr)O_2$ in individual samples as obtained from the Rietveld refinement (interconnected symbols) and as calculated for a mixture of stoichiometric phases $Cr_2O_3$ and $ZrO_2$ according to Eq. (3) (dotted lines). Below 900°C, the results of the phase analysis are not shown, because the samples Zr8CrO and Zr15CrO were amorphous in this

temperature range. Sample Zr3CrO contains less than 1 mol % t-$(Zr,Cr)O_2$ prior to annealing at 900°C.

Figure 7: Stress-free lattice parameters of hexagonal $(Cr,Zr)_2O_3$ (open symbols) and the changes of the lattice parameters calculated for a constant thermal expansion in the whole temperature range (solid and dashed lines). The lattice parameters indicated by solid lines were calculated for expanded elementary cell of $(Cr,Zr)_2O_3$ in sample Zr3CrO, the lattice parameters indicated by dashed line for the intrinsic lattice parameter of $Cr_2O_3$.

Figure 8: Thermal expansion coefficients calculated from the stress-free lattice parameters shown in Fig. 7. The dashed lines indicate the asymptotic values of the thermal expansion coefficients determined for sample Zr3CrO as described in text.

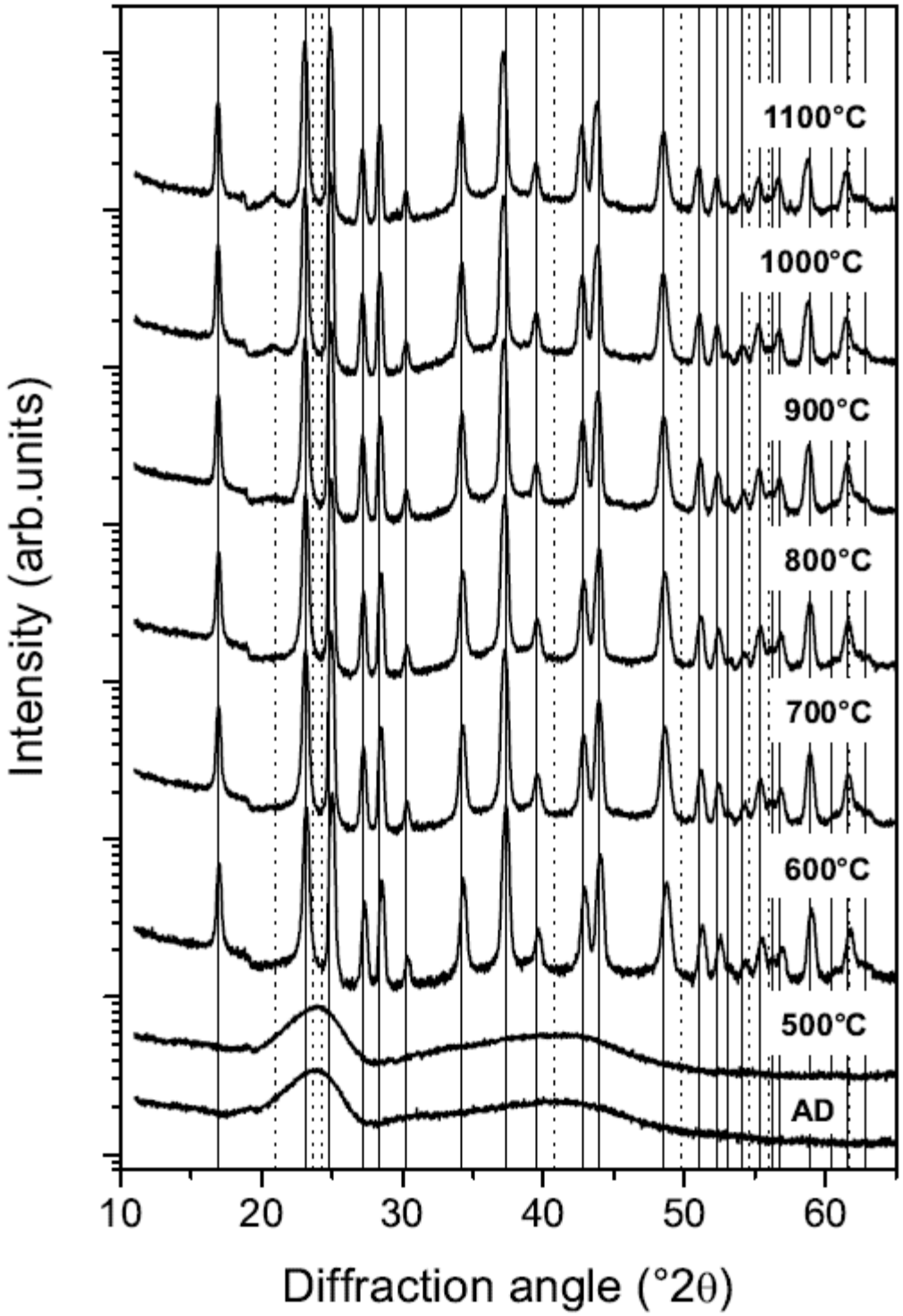
1100°C
1000°C
900°C
800°C
700°C
600°C
500°C
AD
Intensity (arb.units)
10
20
30
40
50
60
Diffraction angle (°2θ)

Figure 1

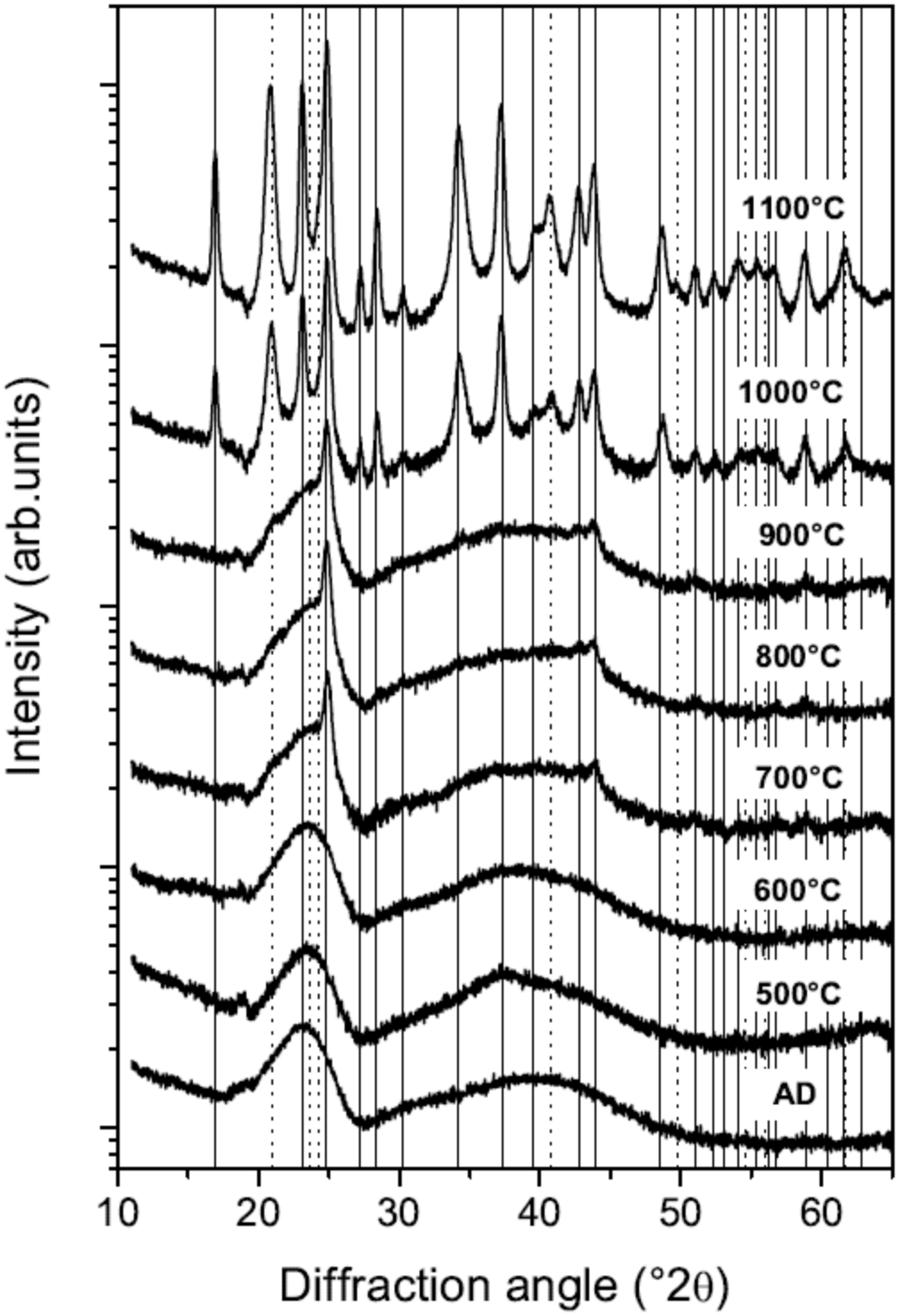
1100°C
1000°C
900°C
800°C
700°C
600°C
500°C
AD
Intensity (arb.units)
10
20
30
40
50
60
Diffraction angle (°2θ)

Figure 2

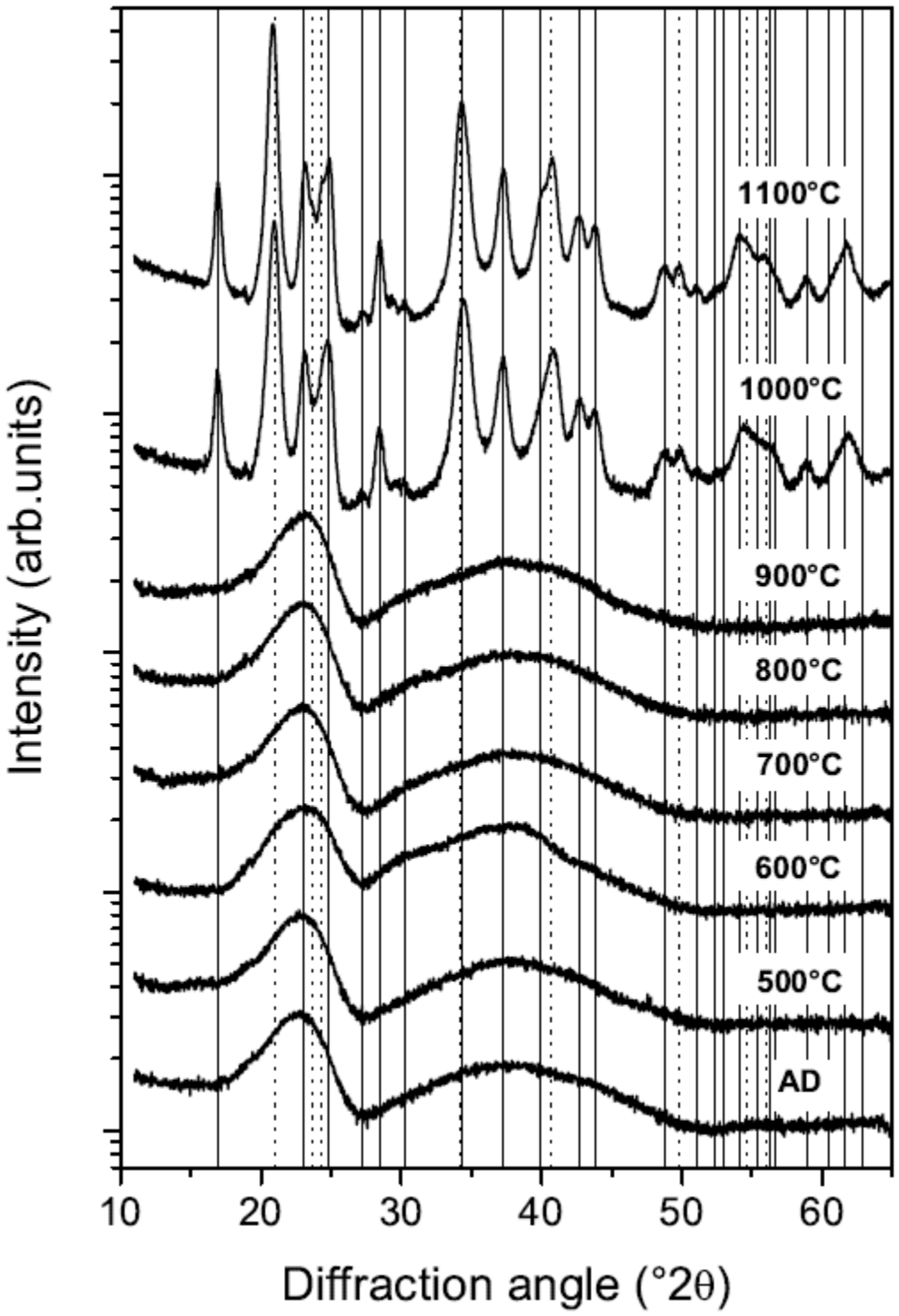
1100°C
1000°C
900°C
800°C
700°C
600°C
500°C
AD
Intensity (arb.units)
10
20
30
40
50
60
Diffraction angle (°2θ)

Figure 3

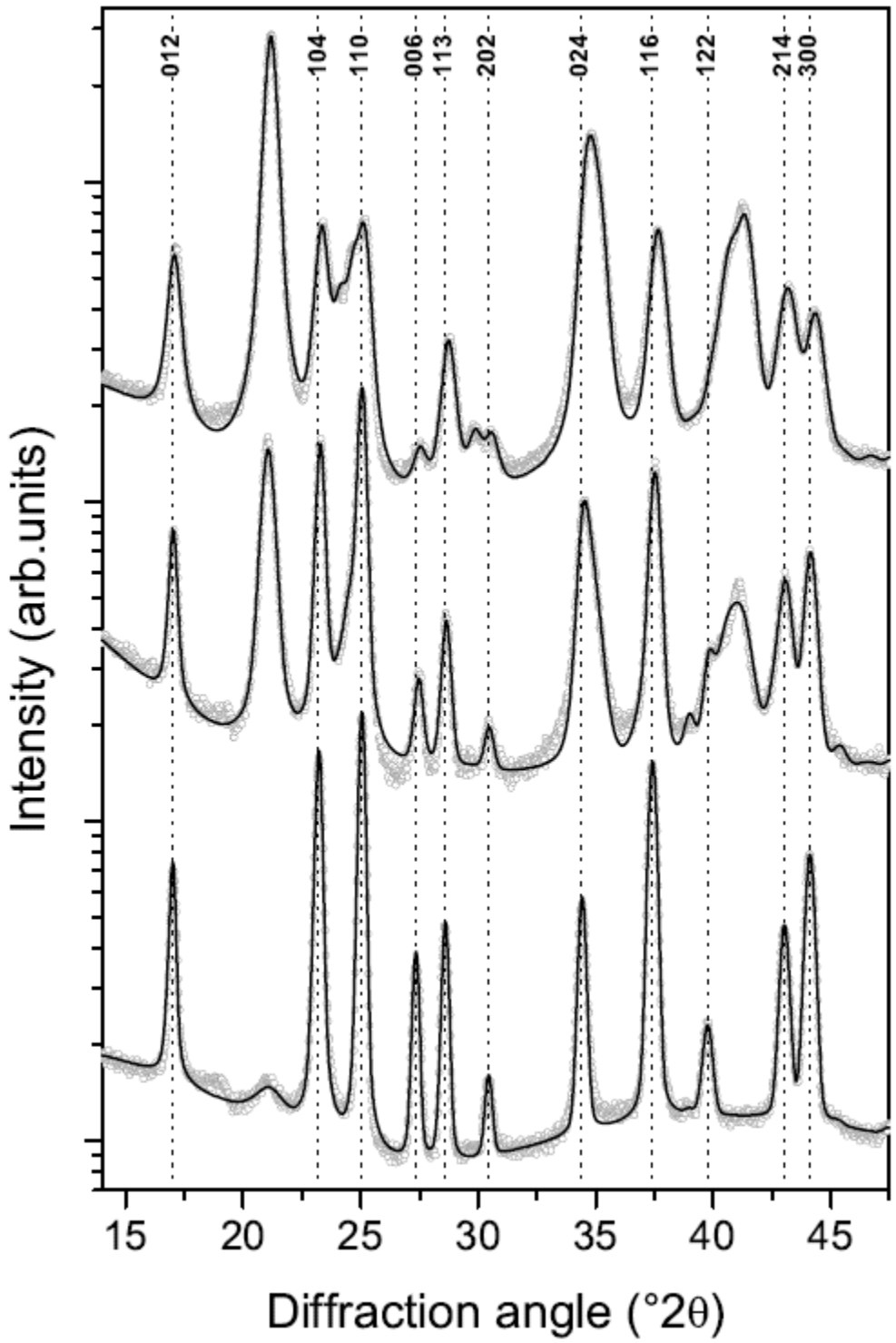
012
104
110
006
113
202
024
116
122
214
300
Intensity (arb.units)
15
20
25
30
35
40
45
Diffraction angle (°2θ)

Figure 4

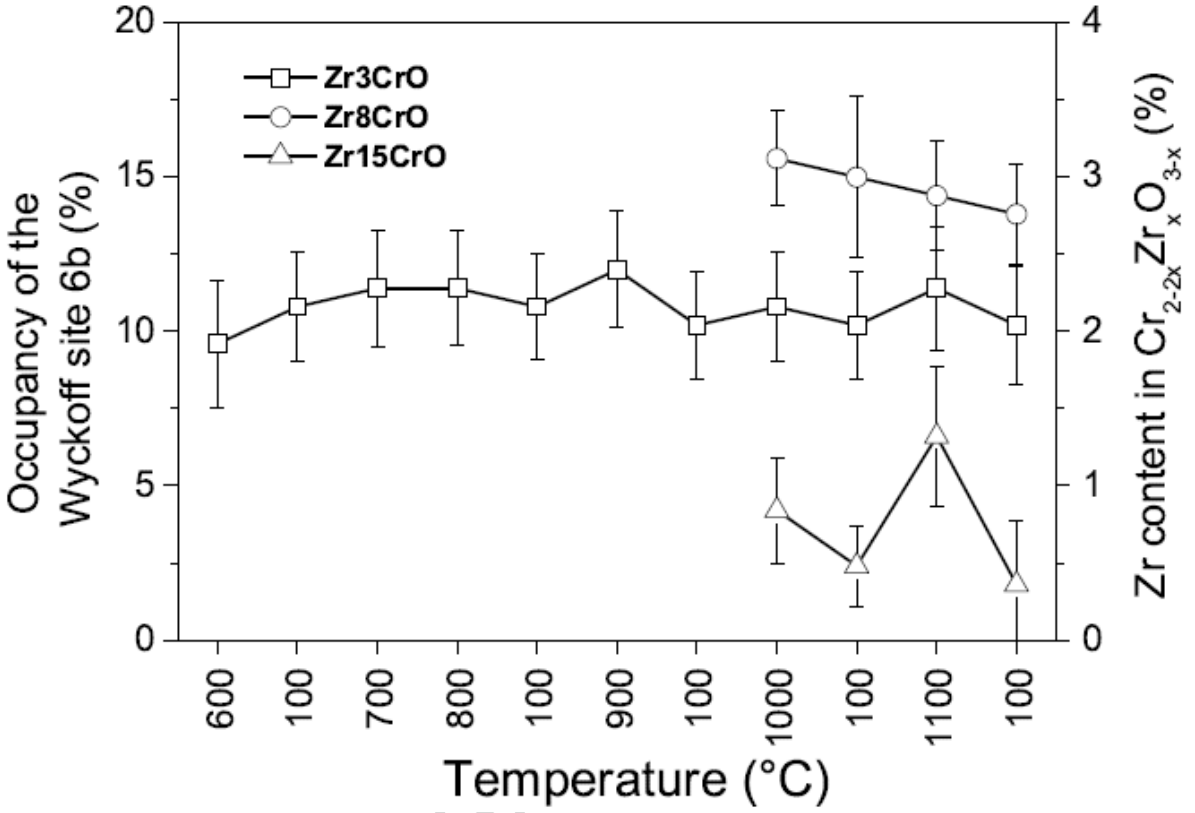


Figure 5

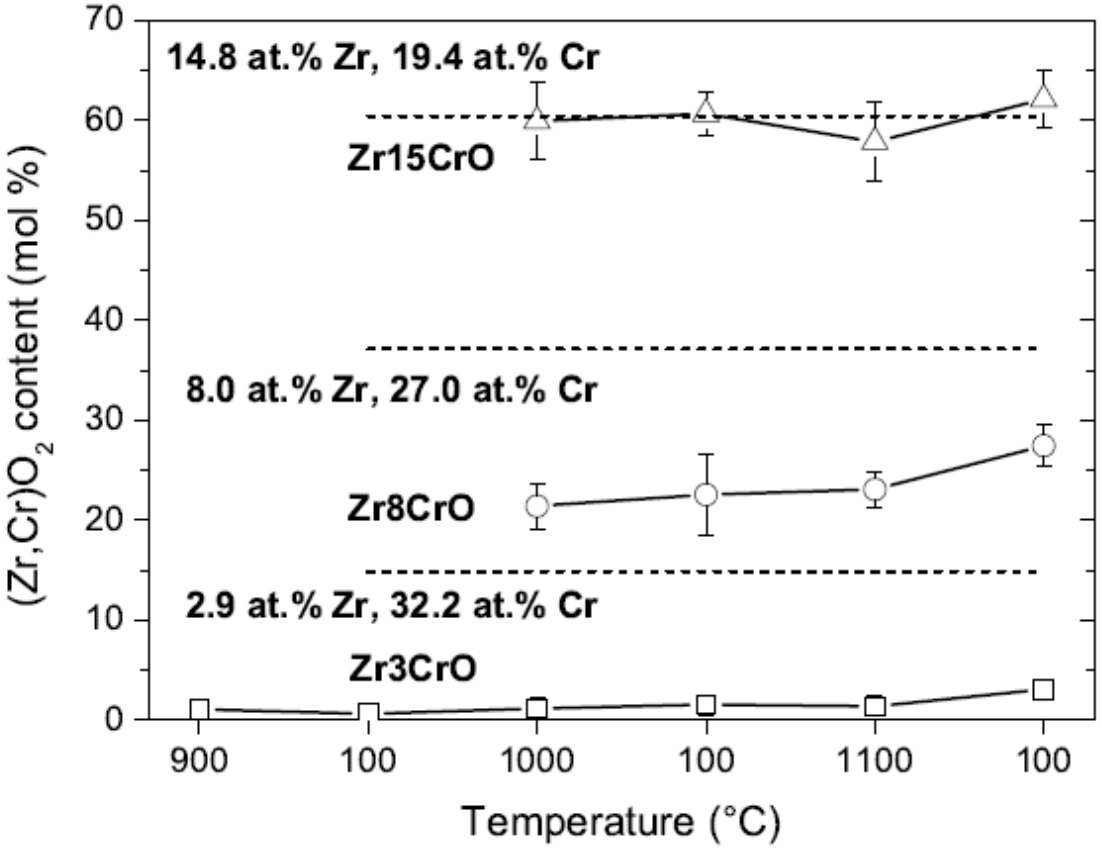


Figure 6

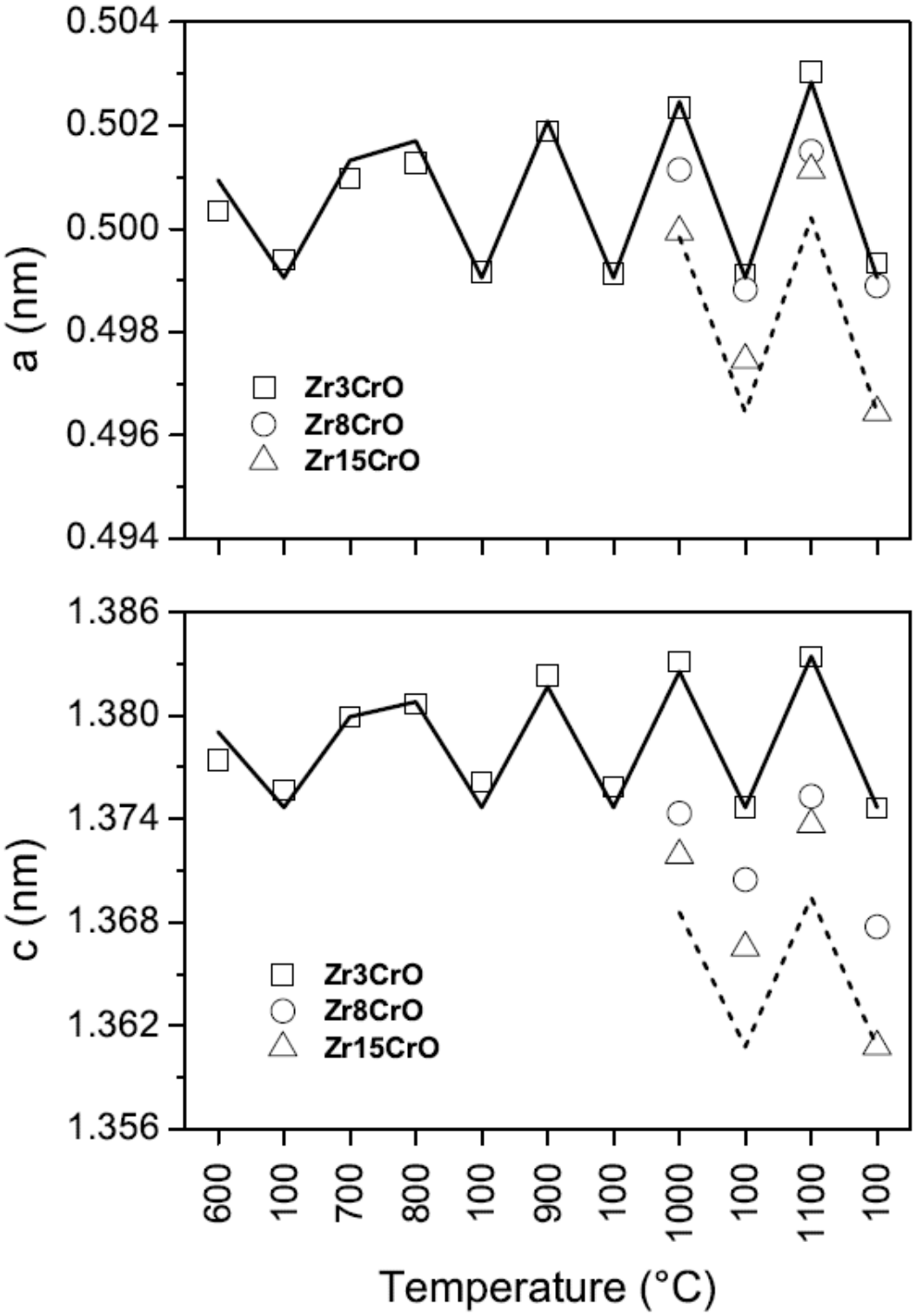


Figure 7

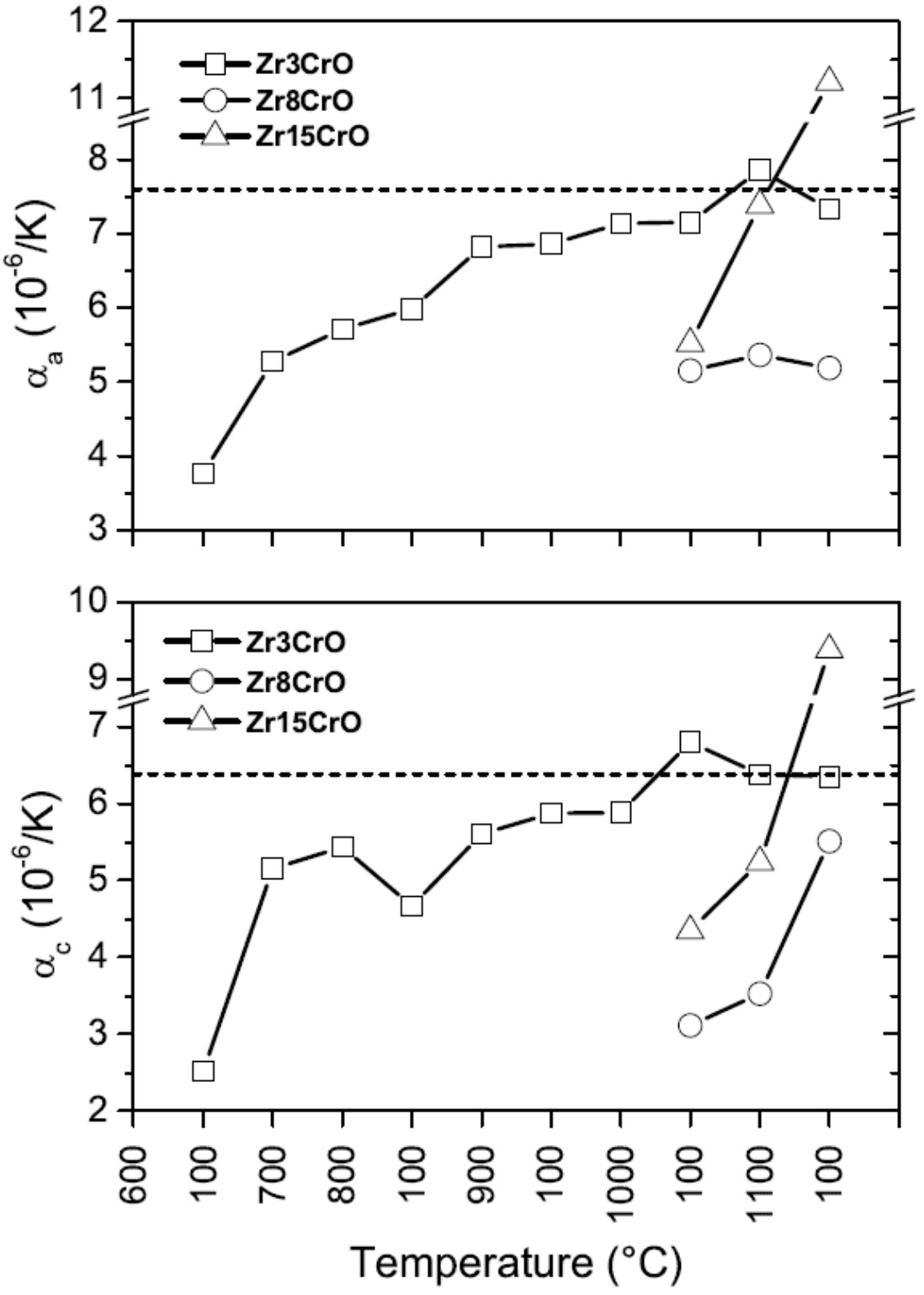


Figure 8

Highlights

- Amorphous Cr-Zr-O thin films were deposited using reactive ion beam sputtering.
- After annealing in vacuum, metastable $(Cr,Zr)_2O_3/(Zr,Cr)O_2$ nanocomposites form.
- The crystallization temperature depends strongly on the Zr concentration.
- Metastable hexagonal $(Cr,Zr)_2O_3$ accommodates up to 3.2 at.% of zirconium.
- Zirconium oxide crystallizes in tetragonal form, as it is stabilized by chromium.